

# Scalable Surface-Based Manipulation Through Modularity and Inter-Module Object Transfer

Pratik Ingle, Jørn Lambertsen, Kasper Støy, Andres Faiña

IT University, Denmark  
{prin, jrnl, ksty, anfv}@itu.dk

**Abstract**—Robotic Manipulation Surfaces (RMS) manipulate objects by deforming the surface on which they rest, offering safe, parallel handling of diverse and fragile items. However, existing designs face a fundamental tradeoff: achieving fine control typically demands dense actuator arrays that limit scalability. Modular architectures can extend the workspace, but transferring objects reliably across module boundaries on soft, continuously deformable surfaces remains an open challenge. We present a multi-modular soft manipulation platform that achieves coordinated inter-module object transfer and precise positioning across interconnected fabric-based modules. A hierarchical control framework, combining conflict-free Manhattan-based path planning with directional object passing and a geometric PID controller, achieves sub-centimeter positioning and consistent transfer of heterogeneous objects including fragile items. The platform employs shared-boundary actuation, where adjacent modules share edge actuators, reducing the required count from  $4n^2$  to  $(n+1)^2$  for an  $n \times n$  grid; a  $2 \times 2$  prototype covers  $1 \times 1$  m with only 9 actuators. This scaling comes at a cost: shared actuators mechanically couple neighbouring modules, creating interference during simultaneous manipulation. We systematically characterise this coupling across spatial configurations and propose compensation strategies that reduce passive-object displacement by 59–78%. Together, these contributions establish a scalable foundation for soft manipulation surfaces in applications such as food processing and logistics.

**Index Terms** – Soft Robot, Robotic Manipulation Surface, Distributed

## I. INTRODUCTION

In domains such as food processing, logistics, and warehouse automation, large numbers of heterogeneous and often fragile objects must be repositioned across extended work areas. Pick-and-place manipulators address this by grasping objects sequentially, but they risk damaging delicate items, struggle with irregular geometries, and are inherently limited in throughput when many objects must move simultaneously. Conveyor belts offer high throughput but are limited to unidirectional transport and cannot reposition objects to arbitrary locations. Robotic Manipulation Surfaces (RMS) offer a fundamentally different strategy: rather than grasping objects directly, they manipulate them by dynamically deforming or actuating the surface on which the objects rest. The distributed contact provided by such surfaces enables safe, parallel handling of diverse objects; including fragile items like eggs and fruits without requiring object-specific end-effectors. These properties make RMS especially attractive for applications that demand high throughput, gentle handling, and operation over large surface areas. However,

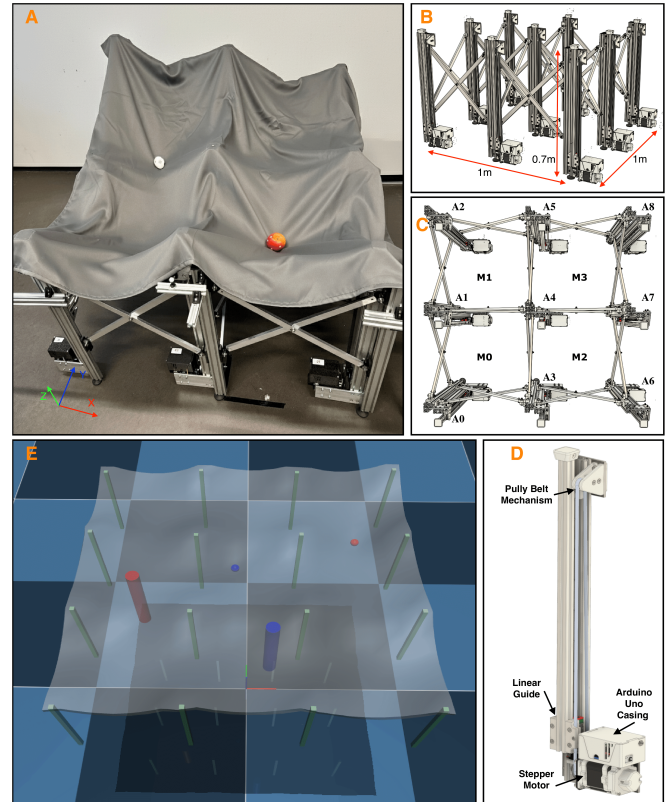


Fig. 1: Multi-modular soft manipulation. (A) Manipulation of an egg and an apple. (B) Side view showing the platform dimensions of  $1 \times 1 \times 0.7$  m (length, width, and height at rest). (C) Top view illustrating the arrangement of nine actuators (A0–A8) and four modules (M0–M3) without the flexible surface. (D) Each linear actuator has 0.4-meter vertical range and built using a stepper motor and pulley-belt mechanism, controlled by an *Arduino Uno* micro controller. (E) MuJoCo simulation of the extended  $3 \times 3$ -module configuration showing two objects (red and blue spheres) and their respective target locations.

realizing these advantages at practical scales remains an open challenge, as existing RMS designs face a fundamental tension between manipulation capability and actuator complexity.

A variety of RMS architectures have been proposed, each

navigating this tradeoff differently. Wheel-based systems [1] use arrays of omnidirectional rollers to transport objects efficiently but require continuous contact and struggle with small or geometrically irregular items that cannot maintain stable engagement with the rollers. Piston-based arrays [2] offer precise, localized control by independently actuating dense grids of vertical pins, enabling both translation and rotation of objects. However, their fine-grained manipulation comes at the cost of high actuator density. ArrayBot [3], for instance, employs a  $16 \times 16$  array of 256 actuators which increases mechanical complexity, fabrication cost, and control overhead as the workspace grows. Alternative approaches based on vibrating plates, airflow levitation, cilia-inspired actuators and deformable gel layers [4], [5] each exploit different physical principles for object transport, but remain constrained by trade-offs in payload capacity, object versatility, or the ability to scale to larger work areas. Across these designs, a common pattern emerges: achieving fine manipulation control typically demands high actuator density, which in turn limits practical scalability. Conversely, designs that reduce actuator count sacrifice the ability to handle diverse objects or achieve precise positioning. Breaking this coupling between manipulation capability and actuator complexity is essential for deploying RMS in real-world, large-area applications.

Chih-Han et al. [6] took a step toward addressing this trade-off with Morpho, a modular self-deformable robot that uses membrane-based surface deformation for inter-module object transfer, though its focus remained on global shape morphing rather than precise manipulation. More recent work, [7] proposed MANTA-RAY a fabric-based manipulation platform that directly targets the density–capability coupling by using a soft polyester fabric surface supported by only four corner-mounted linear actuators. Despite this drastically reduced actuator count, a single module achieves an object-to-actuator size ratio as low as 0.01 and successfully manipulates fragile and heterogeneous objects such as eggs and fruits using a simple geometric transformation-based PID controller without requiring learning-based methods. However, these results have been demonstrated only on a single module with a fixed workspace ( $0.5 \times 0.5$  m). Extending to multiple modules introduces two challenges that do not arise in the single-module case: transferring objects reliably across module boundaries where the continuous fabric surface deforms unpredictably, and managing the mechanical coupling that arises when neighbouring modules share physical actuators. Neither challenge has been addressed for soft manipulation surfaces.

Extending MANTA-RAY approach to multiple modules is not a straightforward replication of the single-module design. Naïvely placing independent four-actuator modules side by side would require  $4n^2$  actuators for an  $n \times n$  grid, reintroducing the high density the original platform was designed to avoid. We instead propose a shared-actuator architecture where adjacent modules share edge actuators, reducing the count to  $(n+1)^2$ , yielding 9 instead of 16 actuators for a  $2 \times 2$  grid (44% reduction), with savings approaching

75% asymptotically. However, this efficiency introduces mechanical coupling: shared actuators serve multiple modules simultaneously, constraining inter-module independence during parallel manipulation. Furthermore, transferring objects across module boundaries requires coordination strategies beyond the single-module controller. Addressing these coupled challenges demands both a compatible modular hardware design and a hierarchical control framework neither of which existed for soft manipulation surfaces prior to this work. We used a  $2 \times 2$  module layout to study these effects in more detail.

In this work, we present a multi-modular platform and make three contributions: (1) a hierarchical control framework that achieves, reliable inter-module object transfer on a soft deformable surface, combining conflict-free Manhattan-based path planning with directional passing and geometric PID control to enable seamless manipulation across interconnected modules including parallel multi-object handling; (2) a systematic experimental characterisation of the interference created by shared actuators, quantifying how coupling scales with neighbourhood topology and proposing compensation strategies that reduce passive-object displacement by 59–78%; and (3) a shared-boundary hardware architecture in which adjacent modules share edge actuators, achieving  $(n+1)^2$  actuator scaling and realised as a reconfigurable  $2 \times 2$  prototype covering  $1 \times 1$  m with only 9 actuators. We validate the system through hardware experiments on seven heterogeneous objects and MuJoCo simulations on  $3 \times 3$  module configurations.

## II. MULTI-MODULAR PLATFORM

### A. Design Concept and Scaling Architecture

The single-module MANTA-RAY platform manipulates objects on a soft fabric surface using four corner-mounted vertical linear actuators that tilt and deform the surface to induce object motion through three mechanisms: rolling, sliding, and pulling [7]. To extend this to larger workspaces, we arrange actuators in an  $(n+1) \times (n+1)$  grid, forming  $n \times n$  modules that share boundary actuators with their neighbours. For a  $2 \times 2$  configuration (Fig. 1C), nine actuators (A0–A8) define four modules (M0–M3), where adjacent modules share two actuators (e.g., A3 and A4 between M0 and M2) and diagonal modules share one (A4 between M0 and M3). This shared-boundary architecture requires only  $(n+1)^2$  actuators instead of the  $4n^2$  needed by independent modules, reducing actuator count by 44% at the  $2 \times 2$  scale with savings approaching 75% asymptotically. Each actuator operates as an independent unit, providing robustness to individual faults.

The multi-modular platform harnesses the same three manipulation mechanisms: rolling, sliding, and pulling scaled across interconnected modules. Rolling and sliding are particularly leveraged for transferring objects between neighbouring modules, while each module retains independent manipulation capability. The efficiency of manipulation depends on the interplay between object geometry and fabric properties such as friction, elasticity, and surface tension.

## B. Hardware Implementation

The physical 2×2 prototype (Fig. 1A–D) consists of nine linear actuators connected by a scissor mechanism that enables adjustable actuator spacing for different workspace requirements. For the experiments in this work, actuators are spaced 0.5 m apart, resulting in a platform size of 1×1 m with a resting height of 0.7 m. Each actuator provides a 0.4 m vertical stroke using a stepper motor (Nema 23 Bipolar, 1.8° step angle, 1.85 Nm holding torque) that converts rotational motion to linear displacement through a pulley-belt mechanism, mounted on a linear guide for smooth travel. Actuators are controlled by Arduino Uno microcontrollers with CNC V3 shields and A4988 stepper drivers, with real-time position feedback from AS5600 magnetic encoders (12-bit resolution). A proportional controller on each Arduino converts desired actuator positions to motor speed commands.

The manipulation surface is a 1.2×1.2 m sheet of 100% polyester fabric, with each module covered by a 0.6×0.6 m section that facilitates surface draping between actuator attachment points. Object tracking is performed by a six-camera OptiTrack system at up to 120 Hz. By modulating the relative heights of the nine actuators, the system generates controlled surface gradients that guide object motion across the fabric through coordinated tilting and deformation.

## III. METHODS

The following sections describe the simulation environment (III-A) and the control formulation (III-B) for the multi-modular platform.

### A. Simulation Setup:

MuJoCo [8] was used as a physics-based simulator, with deformable fabric modeled using flexcomp composite elements. The simulation includes 3×3 module configurations with positional actuators (range  $[\pm 0.20]$  m) spaced 0.5 m apart and a soft fabric surface mimicking the hardware system. The simulation runs at 1000 Hz (Fig. 1E).

### B. Controller

The multi-modular platform achieves object manipulation through two core control modes. The primary challenge is inter-module object passing, which transfers objects across module boundaries by coordinating actuator motions on a continuously deformable surface. Once an object reaches its target module, a local position controller handles fine manipulation within that module. Both rely on geometric deformation principles combined with closed-loop feedback, maintaining a low-dimensional (2D) control space at a control frequency of 10 Hz.

1) *Object Passing*: Objects are transferred between modules using rolling or sliding behaviors, depending on their shape, size, and weight. To induce these behaviors, actuators belonging exclusively to the current module (i.e., not shared with the neighboring module) are raised, while the remaining four actuators; two shared and two belonging to the adjacent module are lowered. This coordinated actuation creates a

temporary local slope that allows the object to roll, slide, or exhibit a combination of both for smooth transfer across module boundaries.

The passing process operates hierarchically (Algorithm 1): a high-level Manhattan-based planner determines the module sequence, while a low-level layer executes each transfer through timed actuator adjustments with real-time OptiTrack feedback and adaptive retries.

---

### Algorithm 1 Object Passing Between Modules

---

**Require:** Object position  $\mathbf{p}$ , target position  $\mathbf{p}_d$ , direction  $dir \in \{\text{center, left, right}\}$ , tracker feedback

**Ensure:** Successful inter-module transfer

```

1:  $m_{\text{curr}} \leftarrow \text{DetectModule}(\mathbf{p})$ ,  $m_{\text{target}} \leftarrow$ 
    $\text{DetectModule}(\mathbf{p}_d)$ 
2: while  $m_{\text{curr}} \neq m_{\text{target}}$  do
3:    $\text{path} \leftarrow \text{FINDPATH}(m_{\text{curr}}, m_{\text{target}})$ 
4:   for each  $(m_{\text{from}}, m_{\text{to}}) \in \text{path}$  do
5:      $\text{act} \leftarrow \text{GETACTUA-}$ 
    $\text{TORSTORAISE}(m_{\text{from}}, m_{\text{to}}, dir)$ 
6:     Raise  $\text{act}$  in  $m_{\text{from}}$  opposite to  $m_{\text{to}}$ 
7:     if  $dir = \text{left}$  then
8:       Raise inner shared actuator (toward A4)
9:     else if  $dir = \text{right}$  then
10:      Raise outer shared actuator (away from A4)
11:    else
12:      Raise both shared actuators equally
13:    end if
14:    Lower remaining actuators to form slope
15:    Hold for  $t_{\text{raise}}$ , then settle for  $t_{\text{settle}}$ 
16:    Update  $\mathbf{p}$ ,  $m_{\text{curr}} \leftarrow \text{DetectModule}(\mathbf{p})$ 
17:    if  $m_{\text{curr}} \neq m_{\text{to}}$  then
18:      Increase  $h_{\text{raise}}$  and  $t_{\text{raise}}$  for retry
19:    end if
20:  end for
21: end while
22: return success

```

---

In Algorithm 1,  $\mathbf{p}$  and  $\mathbf{p}_d$  denote the current and target object positions, while  $m_{\text{curr}}$  and  $m_{\text{target}}$  represent the corresponding source and destination modules.  $\text{DetectModule}()$  identifies the module containing the object, and  $\text{FindPath}()$  computes the shortest module sequence via a Manhattan-based planner that enforces conflict-free paths: when multiple objects are manipulated simultaneously, their planned module sequences are guaranteed not to intersect, ensuring that actively manipulated objects don't occupy same modules. This prevents interference.  $\text{GetActuatorsToRaise}()$  selects actuators to elevate based on the transfer direction and module pair. The direction parameter  $dir$  controls the lateral passing path: raising the inner shared actuator (toward A4) produces a left path, raising the outer shared actuator yields a right path, and raising both equally produces a center path, corresponding to the three transfer trajectories validated in Section IV-B. If the object fails to reach the next module,  $h_{\text{raise}}$  and  $t_{\text{raise}}$  are

adaptively increased for retry.

2) *Position Control*: When both the object and target lie within the same module, a local PID-based controller governs the four actuators supporting the soft surface. Each module forms a rectangular workspace of size  $m \times n$  m, providing four degrees of freedom (DOF) for deformation. The controller takes as input the desired target position  $\mathbf{p}_d = (x_d, y_d)$ , the current object position  $\mathbf{p} = (x, y)$ , actuator base coordinates  $\{(x_i, y_i)\}_{i=1}^4$ , and a reference height  $z_0 = 1.5$  m, following the Manhattan controller in [9].

At each control step ( $f = 10$  Hz), positional errors  $e_x, e_y$  are processed by a PID controller to compute surface tilt angles  $\theta_{zx}$  and  $\theta_{zy}$  about the  $X$ - and  $Y$ -axes. The surface orientation is represented by the normal vector

$$\vec{n} = (\sin \theta_{zx}, \sin \theta_{zy}, \cos \theta_{zx}), \quad (1)$$

which defines the plane

$$\vec{n} \cdot (\vec{r} - \vec{r}_0) = 0, \quad \vec{r}_0 = (0, 0, z_0). \quad (2)$$

The desired actuator heights are then derived from the plane geometry as

$$z_i = \frac{z_0 n_z - n_x x_i - n_y y_i}{n_z}, \quad (3)$$

with corresponding actuator commands

$$a_i = (z_0 - z_i) + \alpha \delta_i, \quad \delta_i \sim U(-1, 1), \quad (4)$$

where the noise term  $\alpha \delta_i$  introduces small vibrations to reduce static friction and enhance object mobility. Each actuator operates within a range of  $[-0.2, 0.2]$  m, allowing a maximum surface tilt of approximately  $\pm 38^\circ$ . Continuous updates of tilt angles and actuator positions ensure smooth, real-time manipulation.

For multi-module operation, neighboring modules share boundary actuators that are jointly controlled to form localized gradients for object transfer. This distributed approach maintains the simplicity and low-dimensionality of the single-module controller while enabling seamless, large-scale manipulation across the deformable fabric surface.

## IV. RESULTS

To evaluate the proposed platform, we conducted five sets of experiments on the  $2 \times 2$  hardware prototype. The first three experiments, *Object Passing*, *Directional Passing*, and *Target Reaching*, collectively demonstrate reliable inter-module object transfer on a soft deformable surface for the first time, characterising transfer repeatability, directional control, and cross-module positioning accuracy. The remaining two experiments, *Multi-Object Manipulation* and *Influence on Neighbouring Module*, evaluate the consequences of shared-boundary actuation for parallel operation. We validate scalability through MuJoCo simulations on  $3 \times 3$  module configurations.

### A. Object passing

During object passing, the rolling and sliding behaviors depend strongly on the object's shape and surface characteristics. The more irregular the object, the more distinct and variable its motion becomes during transfer. To evaluate transfer repeatability, each of six objects (Table I) was passed from the center of module M0 to adjacent module M2 and back, repeated three times. Figure 2 presents the resulting trajectories, with vertical lines indicating module boundary crossings.

Spherical objects such as the apple (Fig. 2a) and sphere (Fig. 2b) exhibited consistent rolling behavior, while the disk showed repeatable sliding due to its large contact area and low center of gravity. In contrast, the cube (Fig. 2f) and dice (Fig. 2c) displayed greater variability across runs: the cube rolled in multiple discrete steps, whereas the dice tended to roll in single steps, reflecting differences in size and weight. The cylindrical object exhibited both rolling and sliding depending on its orientation, with greater variability when misaligned. Overall, smoother symmetric objects produced stable repeatable trajectories, while irregular geometries increased variability in both lateral and vertical motion. The mean positional deviation across all objects remained within 0.03 m, confirming consistent inter-module transfer performance.

### B. Directional Passing

We investigated how the lateral position of object transfer, whether along the center, left, or right path relative to the passing direction affects manipulation performance. In this experiment, various objects were passed between neighbouring modules along a square trajectory (anticlockwise: M0→M2→M3→M1) across the surface. Each object followed three square paths in a continuous loop of two cycles: a *normal square* (blue), where the object passed through the center between shared actuators; a *small square* (purple), where the transfer occurred closer to the central actuator (A4); and a *large square* (yellow), where the object was passed farther from the central actuator (A4). Ideally, during object passing an object should move along the central path between the shared actuators, forming a perfect square trajectory as shown by the dotted red line in Fig. 3, representing the normal square. When the central actuator is raised during object passing, the object traces a larger square path, whereas raising the outer actuator between shared modules results in a smaller square path. In practice, the trajectories deviate slightly for normal squares due to the fabric's elasticity and tension distribution. Spherical objects such as the sphere and egg produced three clearly distinguishable paths corresponding to the three square sizes, while the cube primarily followed the central trajectory between shared actuators. These results demonstrate that the passing direction can be actively controlled by selecting which boundary actuator to raise, enabling center, left, or right transfer paths relative to the shared actuator pair.

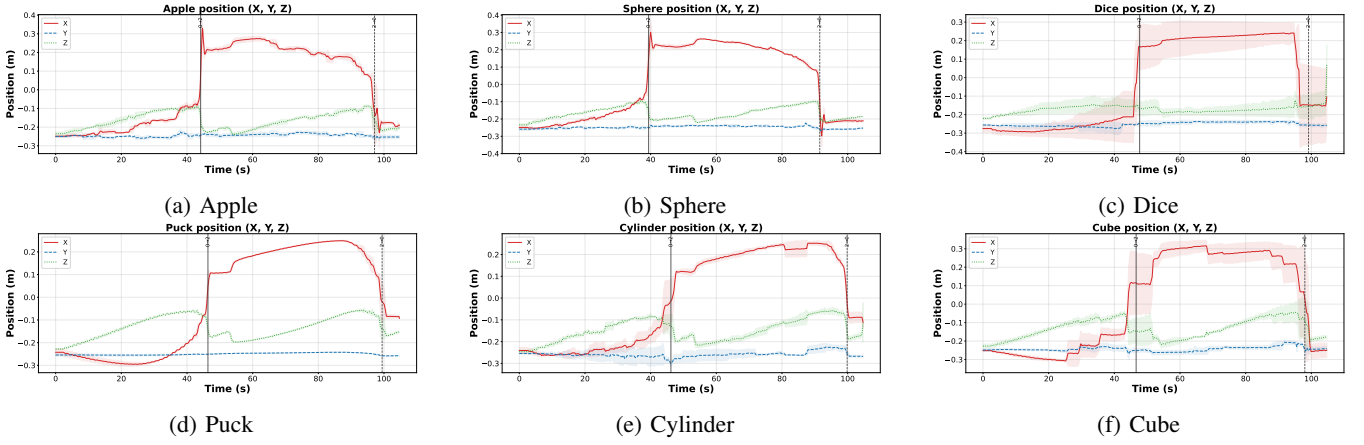


Fig. 2: Object Passing from M0 to M2 and back from M2 to M0

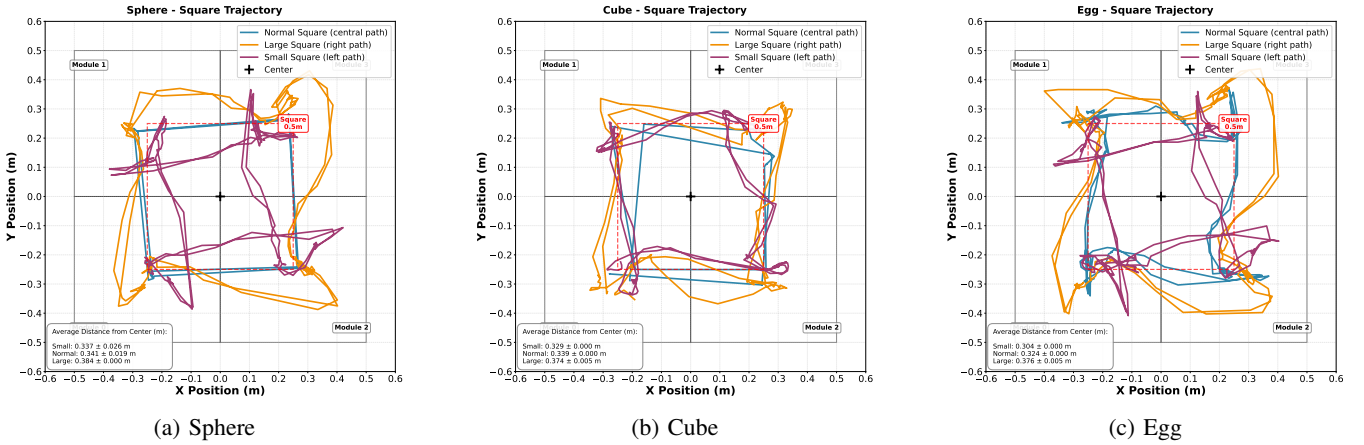


Fig. 3: Three square paths (anticlockwise: M0→M2→M3→M1) of the object: Normal square (central direction, Blue), Small square (left direction, Purple) and Large square (right direction, Orange)

### C. Target reaching

Target reaching evaluates end-to-end manipulation performance, combining inter-module transfer with local position control. We performed a target-reaching experiment with seven heterogeneous objects listed in Table I to evaluate the precision of manipulation; four representative cases are shown in Fig. 4. Each object was placed at an initial position (green circle) and tasked to reach a target location (red star) within a threshold radius of 0.03 m (red circle). If the object’s initial module differed from the target module, it was first transferred along a Manhattan path to the appropriate module. Once on the target module, the position controller was activated to achieve precise alignment within the specified boundary.

Figure 4 shows that all objects successfully reached their respective target positions within the defined threshold on  $2 \times 2$  hardware module. Elongated objects, such as the egg (Fig. 4c) and the cylinder (Fig. 4d), reached the target but required small corrective zig-zag motions to fine-tune their final positions. In contrast, spherical objects achieved smoother and more direct trajectories, demonstrating higher positional stability and control precision. Overall, the system

achieved a mean positioning error of less than 0.02 m across all trials, confirming the controller’s reliability in handling heterogeneous objects.

### D. Multi-Object Manipulation

To evaluate the scalability and distributed coordination capability of the multi-modular platform, we conducted experiments involving simultaneous manipulation of two objects, a disk and a sphere on the  $2 \times 2$  modular hardware platform. In this setup, each module operated its local controller independently, allowing parallel actuation and position control without centralized coordination. Objects were placed on different modules, a sphere on M3 and Disk on M0 and tasked to reach individual target locations M1 and M3 respectively.

Figure 5a shows the trajectories of a sphere and a disk manipulated concurrently across separate modules. The results demonstrate that the distributed control scheme enables stable and synchronized motion across modules. The platform maintained consistent tracking performance and each object reached its target within the 0.03 m positional threshold. The conflict-free Manhattan path planner ensures that the two objects never occupy same modules simultaneously,

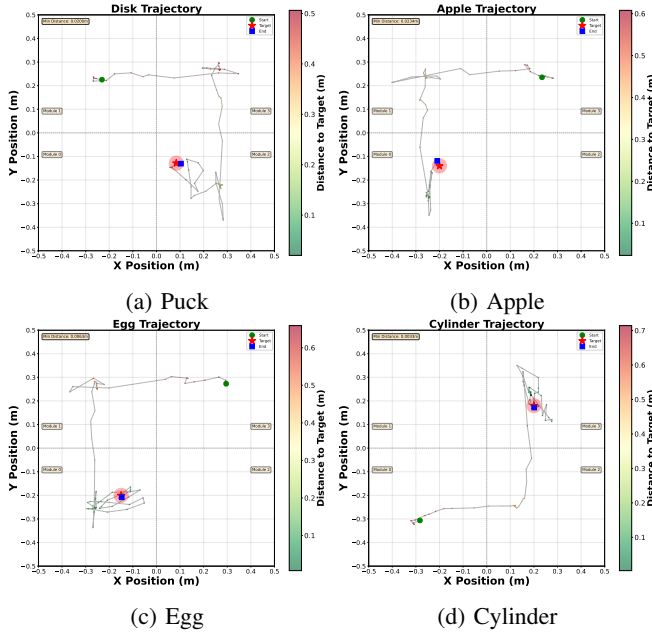


Fig. 4: Target reaching for different objects on hardware platform. Object start at initial position (green circle) and move to target location (red star) within a threshold of 3 cm (red circle) along the line path.

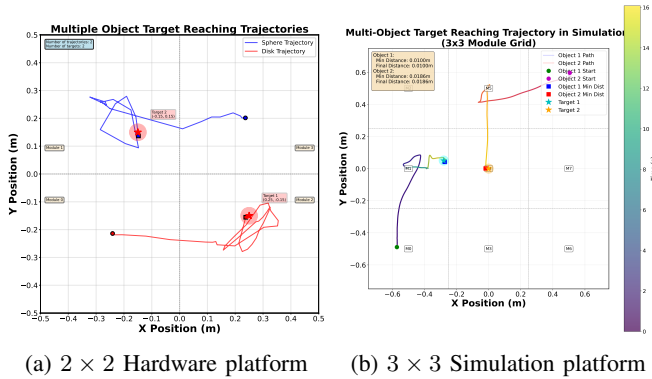


Fig. 5: Multi-object target reaching demonstrated on the multi-module platform: (a) hardware implementation, (b) simulation on a  $3 \times 3$  modular configuration.

avoiding interference. We also verified scalability of the platform in simulation by performing multi-object target reaching on a  $3 \times 3$  platform with two spherical objects (Fig. 5b). These results confirm that the modular actuation framework supports parallel manipulation of heterogeneous objects, achieving sub-3 cm positioning accuracy for both objects simultaneously.

### E. Influence on Neighbouring Module Object

A key consequence of shared-boundary actuation is that manipulating an object on one module perturbs the surfaces of its neighbours. To quantify this interference, we measure the displacement of a stationary object on a passive module while another object is actively manipulated on an adjacent module (Fig. 6). We report three complementary metrics:

Object	Weight (g)	Size (cm)	Fabrication Method
Sphere	32	$\varnothing 4.5$	Molding
Cube	31	$4.2 \times 4.2 \times 4.2$	FDM 3D Printing
Disk	26	$\varnothing 7$ , Thickness: 2.5	FDM 3D Printing
Apple	120.4	$\varnothing 5-7$	–
Cylinder	71.3	$\varnothing 3$ , Height: 13	Clean Spray hand sanitizer
Egg	61.2	$\varnothing(4.1-6.2)$	–
Dice	5	$1.5 \times 1.5 \times 1.5$	Molding

TABLE I: Details of objects: weight, size, and fabrication method.

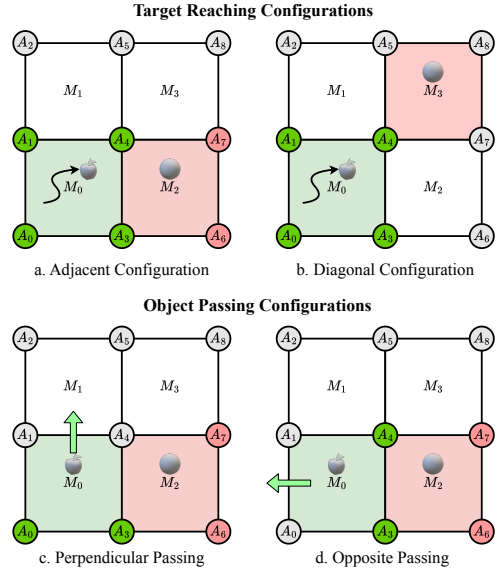


Fig. 6: Spatial configurations for the neighbouring-module interference study ( $2 \times 2$  Module, top view). The manipulated object resides on the active (green) module; the stationary object is tracked on the passive (red) module. For stabilisation in c, red actuators are raised to compensate for shared-actuator coupling.

RMSE<sub>xy</sub> (average displacement over the manipulation duration), maximum displacement  $d_{\max}$  (worst-case perturbation), and final displacement  $d_{\text{final}}$  (permanent drift after manipulation ends). A sphere and puck serve as stationary objects, representing rolling-dominant and sliding-dominant geometries respectively. Two sources of interference are evaluated: target reaching and object passing. All the experiments are repeated three times.

1) *Target Reaching Influence*: We examine two spatial configurations (Fig. 6a,b): *adjacent modules*(4-neighbour), where two actuators are shared between active and passive modules (e.g., A3 and A4 between M0 and M2), and *diagonal modules*(diagonal-neighbour), where only a single actuator is shared (A4 between M0 and M3).

Without compensation, the adjacent configuration produces severe sphere interference (RMSE<sub>xy</sub>: 0.217 m,  $d_{\max}$ : 0.460 m,  $d_{\text{final}}$ : 0.461 m), with the near-equal  $d_{\max}$  and  $d_{\text{final}}$  confirming permanent drift and frequent module exit (Fig. 7). The puck shows lower but substantial sensitivity (RMSE<sub>xy</sub>:

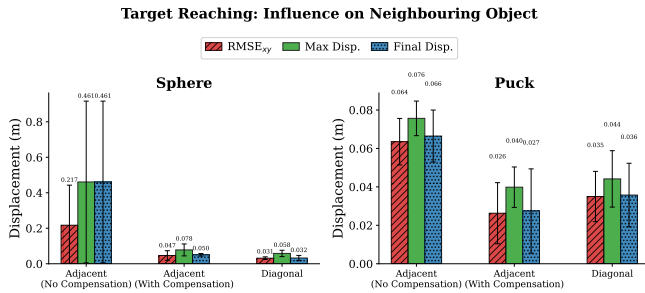


Fig. 7: Target reaching: influence on a stationary neighbouring object. Three displacement metrics reported for adjacent (No compensation and compensation) and diagonal configurations. Left: sphere. Right: puck. Stabilised adjacent performance approaches diagonal levels across all metrics.

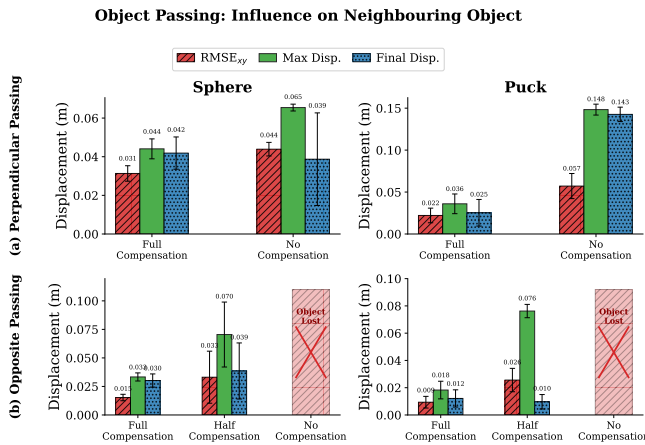


Fig. 8: Object passing: influence on a stationary neighbouring object. (a) Perpendicular passing (one shared actuator active). (b) Opposite passing (both shared actuators active); red crosses indicate object loss without stabilisation. Left: sphere. Right: puck.

0.064 m,  $d_{\max}$ : 0.076 m) due to its flat contact geometry resisting rolling. The diagonal configuration exhibits markedly less coupling (sphere  $RMSE_{xy}$ : 0.031 m, puck: 0.035 m), confirming that interference scales with the number of shared actuators.

To mitigate adjacent interference, we propose a *stabilisation strategy*: the two non-shared actuators (Fig 6, red actuators) of the passive module are raised to 0.35 m. When shared actuators (A3 and A4) are moved during active manipulation on the M0 module, the passive module’s M2 surface develops an unintended tilt toward the active module. Raising the non-shared actuators creates a counter-tilt that maintains a locally level surface, preventing object displacement. This reduces sphere  $RMSE_{xy}$  to 0.047 m (78% reduction),  $d_{\max}$  to 0.078 m, and  $d_{\text{final}}$  to 0.050 m, approaching diagonal level performance. The puck similarly improves to  $RMSE_{xy}$ : 0.026 m (59% reduction),  $d_{\max}$ : 0.040 m (Fig. 7).

2) *Object Passing Influence*: During inter-module transfer, shared actuators are actively raised to create the passing slope, producing a distinct interference profile compared to

TABLE II: Interference summary across all conditions. All displacement values in meters.

Scenario	Obj.	No Compensation			Full Compensation			$\Delta RMSE$
		RMSE	$d_{\max}$	$d_{\text{fin}}$	RMSE	$d_{\max}$	$d_{\text{fin}}$	
Target (Adj.)	Sph.	0.217	0.460	0.461	0.047	0.078	0.050	78%
Target (Adj.)	Puck	0.064	0.076	0.066	0.026	0.040	0.027	59%
Target (Diag.)	Sph.	0.031	0.058	0.032	–	–	–	base
Target (Diag.)	Puck	0.035	0.044	0.036	–	–	–	base
Pass. (Perp.)	Sph.	0.044	0.065	0.039	0.031	0.044	0.042	30%
Pass. (Perp.)	Puck	0.057	0.148	0.143	0.022	0.036	0.025	61%
Pass. (Opp.)	Sph.	Lost	–	–	0.015	0.030	0.030	–
Pass. (Opp.)	Puck	Lost	–	–	0.009	0.018	0.012	–

target reaching. Two passing directions are evaluated relative to the passive module (Fig. 6c,d):

**Perpendicular passing** (Fig. 6c): Object 1 is passed between modules sharing one actuator with the passive module (e.g., M0 to M1 while Object 2 rests on M2). Without stabilisation, moderate interference occurs (sphere  $RMSE_{xy}$ : 0.044 m; puck: 0.057 m). The puck exhibits high  $d_{\max}$  (0.148 m) and  $d_{\text{final}}$  (0.143 m) despite lower  $RMSE_{xy}$ , indicating that once displaced, flat objects do not self-correct. Stabilisation where the non-shared actuators of the passive module mirror the passing action reduces sphere  $RMSE_{xy}$  to 0.031 m and puck to 0.022 m (Fig. 8a).

**Opposite passing**: (Fig. 6d): Object 1 is passed outward from M0, causing both shared actuators (A3, A4) to rise simultaneously. Without compensation, this produces critical interference, with displacement exceeding the module boundary and resulting in complete object loss for stationary object. Two mirroring strategies address this: *full-mirror compensation*, where non-shared actuators (red) match the passing height (green actuators), achieves the lowest displacement (sphere: 0.015 m, puck: 0.009 m); *half-mirror compensation*, at half the passing height, yields intermediate values (sphere: 0.033 m, puck: 0.026 m) while preserving partial actuation freedom on the passive module (Fig. 8b).

Across all conditions (Table II), interference severity scales directly with the number of active shared actuators, and spherical objects are consistently more sensitive than flat objects during target reaching, while flat objects show greater permanent drift during passing. The proposed stabilisation strategies reduce  $RMSE_{xy}$  by 30–78% across configurations, confirming that the coupling inherent to  $(n + 1)^2$  shared-boundary actuation can be effectively managed through actuator compensation.

## V. DISCUSSION

The multi-modular platform demonstrates, for the first time, that objects can be reliably transferred and precisely positioned across interconnected soft fabric modules. The hierarchical control framework achieves this without learning-based methods, using only geometric deformation principles and closed-loop feedback, notable given the fabric’s nonlinear catenary profile and friction-dependent dynamics. The conflict-free Manhattan path planner provides a first layer of interference management by ensuring that simultaneously manipulated objects never occupy same modules.

When interference from adjacent operations is unavoidable, the proposed compensation strategies reduce passive-object displacement by 59–78%, providing a second layer of mitigation at the actuation level. The enabling shared-boundary architecture covers a  $1 \times 1$  m workspace with 9 actuators instead of the 16 that independent modules would require. Beyond this practical hardware reduction, the architecture fundamentally shapes the control problem: the interference study shows that coupling scales directly with the number of shared actuators, with adjacent modules (two shared) experiencing up to 0.217 m passive displacement while diagonal modules (one shared) show only 0.031–0.035 m. This quantitative relationship provides a predictive basis for larger configurations. In a  $3 \times 3$  grid, the central module shares actuators with four neighbours, making interference management increasingly critical. At larger scales, simultaneous manipulation across multiple neighbouring modules can trigger cascading displacements through chains of shared actuators. In such cases, half-mirror compensation can contain the disturbance within a few modules of the active site, as actuator perturbations attenuate across successive shared boundaries and become negligible after two to three modules.

Object geometry plays a dominant role across all experiments, particularly during inter-module transfer. Spherical objects show higher instantaneous sensitivity during target reaching (RMSE<sub>xy</sub>: 0.217 m vs. 0.064 m for the puck), as even small tilts induce rolling. However, during passing, flat objects exhibit greater permanent drift ( $d_{\text{final}}$ : 0.143 m for puck vs. 0.039 m for sphere), indicating that once displaced, flat objects lack a restoring mechanism. This distinction suggests that object-aware control policies, even at a coarse rolling-vs-sliding classification level, could enable tailored compensation strategies for each module and inform the choice of passing parameters during inter-module transfer.

The current system follows Manhattan-path trajectories aligned to module grid axes. Finer within-module trajectory control is constrained by the four-actuator configuration, which provides only two independent tilt axes. Achieving arbitrary paths would require either higher actuator density, contradicting the reduced-density philosophy, or time-varying sequences exploiting fabric dynamics, a promising future direction.

Regarding orientation control, the platform controls object position but not orientation, relevant for high aspect-ratio objects like cylinders and eggs that exhibited corrective zig-zag motions during target reaching. Unlike rigid tilting platforms, the fabric introduces position-dependent coupling between surface shape and object pose. Potential approaches include exploiting asymmetric friction during sequential tilt-and-release motions or rapid oscillatory actuation for dynamic reorientation.

While simulation closely mirrors the hardware and shows good agreement at the  $2 \times 2$  scale, constructing a  $3 \times 3$  prototype remains a priority. The current inter-module transfer strategy relies on open-loop timed actuation phases; closed-loop transfer using real-time object tracking during the passing phase itself could improve reliability for lighter or

more irregular objects. The interference study characterises coupling for two objects; in larger configurations, multi-source interference patterns become combinatorial, requiring decentralised control strategies. Additionally, integrating embedded sensing would reduce reliance on the external OptiTrack system, and adaptive gain tuning based on object type and interference conditions could further improve performance.

## VI. CONCLUSION

This work demonstrated, reliable inter-module object transfer and coordinated manipulation across interconnected soft fabric modules. A hierarchical control framework combining conflict-free Manhattan-based path planning with directional passing and geometric PID control achieves sub-centimeter positioning accuracy, consistent transfer of heterogeneous objects including fragile items, and parallel multi-object manipulation. Interference from shared-boundary actuation is managed through a two-layer approach: conflict-free path planning prevents simultaneously active neighbouring modules, while actuator compensation reduces residual passive-object displacement by 59–78%. The enabling shared-boundary hardware architecture requires only  $(n + 1)^2$  actuators for an  $n \times n$  grid, covering  $1 \times 1$  m with 9 actuators instead of 16 for independent modules. Together, these findings confirm that the coupling inherent to shared-boundary architectures can be effectively addressed without sacrificing manipulation performance, establishing a foundation for deploying soft manipulation surfaces in large-area applications. Future work targets  $3 \times 3$  hardware validation, closed-loop inter-module transfer, and embedded sensing for object-aware manipulation. The structural parallels with physically-coupled multi-agent systems suggest that the platform can also serve as a testbed for studying decentralised coordination in distributed manipulation.

## REFERENCES

- [1] Claudio Uriarte and Hendrik Thamer. Methode zur bewertung der flexibilität und wandelbarkeit am beispiel eines omnidirektionalen fördersystems. *Logistics Journal: Proceedings*, 2022(18), 2022.
- [2] BK Johnson, M Naris, V Sundaram, A Volchko, K Ly, SK Mitchell, E Acome, N Kellaris, C Keplinger, N Correll, et al. A multifunctional soft robotic shape display with high-speed actuation, sensing, and control. *Nature Communications*, 14(1):4516, 2023.
- [3] Zhengrong Xue, Han Zhang, Jingwen Cheng, Zhengmao He, Yuanchen Ju, Changyi Lin, Gu Zhang, and Huazhe Xu. Arraybot: Reinforcement learning for generalizable distributed manipulation through touch. In *2024 IEEE International Conference on Robotics and Automation (ICRA)*, pages 16744–16751. IEEE, 2024.
- [4] Quan Zhou, Veikko Sariola, Kourosh Latifi, and Ville Liimatainen. Controlling the motion of multiple objects on a chladni plate. *Nature communications*, 7(1):12764, 2016.
- [5] Hyungpil Moon and Jonathan Luntz. Distributed manipulation of flat objects with two airflow sinks. *IEEE Transactions on robotics*, 22(6):1189–1201, 2006.
- [6] Chih-Han Yu, Kristina Haller, Donald Ingber, and Radhika Nagpal. Morpho: A self-deformable modular robot inspired by cellular structure. In *2008 IEEE/RSJ International Conference on Intelligent Robots and Systems*, pages 3571–3578. IEEE, 2008.
- [7] Pratik Ingle, Kasper Støy, and Andres Faiña. Soft manipulation surface with reduced actuator density for heterogeneous object manipulation. In *2025 IEEE 8th International Conference on Soft Robotics (RoboSoft)*, pages 1–8, 2025.

- [8] Emanuel Todorov, Tom Erez, and Yuval Tassa. Mujoco: A physics engine for model-based control. In *2012 IEEE/RSJ International Conference on Intelligent Robots and Systems*, pages 5026–5033. IEEE, 2012.
- [9] Pratik Ingle, Kasper Støy, and Andres Faiña. Heterogeneous object manipulation on nonlinear soft surface through linear controller. In *2025 IEEE 21st International Conference on Automation Science and Engineering (CASE)*, pages 1780–1787, 2025.